ORNL/TM-2019/1224

Report on FY19 Testing in Support of Integrated EPP-SMT Design Methods Development

Yanli Wang
Robert I. Jetter
Mark C. Messner
T.-L. Sham

August 9, 2019

OAK RIDGE NATIONAL LABORATORY
MANAGED BY UT-BATTELLE FOR THE US DEPARTMENT OF ENERGY

ORNL/TM- 2019/1224

Materials Science and Technology Division

REPORT ON FY 19 TESTING IN SUPPORT OF INTEGRATED EPP-SMT DESIGN METHODS DEVELOPMENT

Yanli Wang
Robert I. Jetter*
Mark C. Messner†
T.-L. Sham†

* RI Jetter Consulting
†Argonne National Laboratory

Date Published: August 2019

Prepared by
OAK RIDGE NATIONAL LABORATORY
Oak Ridge, TN 37831-6283
managed by
UT-BATTELLE, LLC
for the
US DEPARTMENT OF ENERGY
under contract DE-AC05-00OR22725

CONTENTS

LIST OF FIGURES

LIST OF TABLES

ACRONYMS

ART	Advanced Reactor Technologies Program
ASME	American Society of Mechanical Engineers
B&PV	Boiler and Pressure Vessel
CF	Creep-Fatigue
DOE	Department of Energy
EPP	Elastic-Perfectly Plastic
ORNL	Oak Ridge National Laboratory
SBSMT	Single-Bar Simplified Model Test
SMT	Simplified Model Test

ACKNOWLEDGMENTS

This research was sponsored by the US Department of Energy, Office of Nuclear Energy, under contract No. DE-AC02-06CH11357 with Argonne National Laboratory, managed and operated by UChicago Argonne LLC, and under contract DE-AC05-00OR22725 with Oak Ridge National Laboratory (ORNL), managed and operated by UT-Battelle, LLC. Programmatic direction was provided by the Office of Nuclear Reactor Deployment of the Office of Nuclear Energy.

The authors gratefully acknowledge the support provided by Sue Lesica, Federal Manager, Advanced Materials, Advanced Reactor Technologies (ART) Program, and Gerhard Strydom of Idaho National Laboratory, National Technical Director, ART Gas-Cooled Reactors Campaign.

The authors also wish to thank ORNL staff members C. Shane Hawkins and Seth T. Baird for their technical support and Donald Erdman III and Lianshan Lin for reviewing this report.

ABSTRACT

Experiments in support of the development of the integrated Elastic–Perfectly Plastic (EPP) analysis and Simplified Model Test (SMT) design methodology continued in FY 2019. Major progress was made in the verification of the newly developed two-bar SMT and single-bar SMT (SBSMT) methods by performing tests on Alloy 617 and SS 316H at high temperatures. Comparable results were achieved when the materials were tested under same conditions using both techniques. Because of its simple test configuration, SBSMT was the preferred testing technique used to evaluate elastic follow-up effect and generate data in support of SMT-based design curves. Evaluation of elastic follow-up was started with testing SS 316H at 815°C using SBSMT in this reporting period. As a result of this effort, the basic procedure and test protocol to provide data in support of the development of SMT-based design curves were established.

This report also summarizes recent test results for the pressurization SMT using test articles with key features on Alloy 617 at intermediate strain ranges and at a low temperature of 850°C. Although more test results are needed in order to fully understand the effect of primary load on SMT creep-fatigue (CF) life, the limited test data indicate that the primary load reduced the SMT life at intermediate strain ranges and high temperatures. Recognizing the advantages of the newly developed SBSMT method, a new test geometry was designed to allow the elevation of the primary load effect on SMT CF life with the SBSMT technique.

Additionally, selected tests were performed on SS 316H (heat 101076) to provide basic information about the heat of material. The tests performed included high-temperature tensile, fatigue, creep fatigue, and thermomechanical experiments. The results will be used to support the verification of the material constitutive model developed at Argonne National Laboratory.

1. BACKGROUND

The concept of the integrated Elastic–Perfectly Plastic (EPP) plus Simplified Model Test (SMT) design methodology is to incorporate the SMT data-based approach for creep-fatigue (CF) damage evaluation into the EPP methodology to avoid separate evaluation of creep and fatigue damage, eliminate the requirement for stress classification in current methods, and greatly simplify the evaluation of elevated temperature cyclic service. The goal of this integrated EPP-SMT methodology is to maximize the advantages of both EPP methods and the SMT CF evaluation approach. The EPP methods greatly simplify the design evaluation procedure by eliminating the need for stress classification, which is the basis of the current simplified design rules. The SMT CF evaluation no longer requires the damage interaction, or D diagram, and the combined effects of creep and fatigue are accounted for in the SMT test data since the specimens are designed to replicate or bound the stress and strain redistribution that occurs in actual components when loaded in the creep regime. This integrated EPP-SMT methodology aims to minimize the over-conservatism in the existing CF evaluation procedure using the damage interaction diagram, or D diagram, while properly accounting for localized defects and stress risers.

A detailed plan has been developed and revised for the development of this integrated EPP-SMT methodology (Wang et al., 2016a, 2016b, 2017a, 2018 and Messner, 2018). The key elements in the development of this integrated approach include (1) the development of a SMT based CF evaluation approach, (2) bounding the EPP strain ranges for the SMT test specimens and realistic structural components, (3) the development of the CF design curves with the effect of elastic follow-up, primary load, hold time effect, and multi-axiality, and (4) additional considerations for welds and the environmental effect such as corrosion, thermal aging, and radiation on the CF design life.

The development of SMT-based design curve requires a significant amount of SMT test data. Experimentally, SMT key feature CF testing has been fully developed and successfully tested for Alloy 617, SS316H, SS304H, and Gr. 91 at high temperatures (Wang et al., 2013a, 2014, 2015, 2016a, 2017b, 2017c). The original SMT test articles were sized to include key features of a real structure in terms of elastic follow-up and stress concentrations. The elastic follow-up effects in these test articles were provided through the elastic energy stored in the thicker or the driver section of the specimen. In order to achieve the desired elastic follow-up factors, the length ratios of the driver section to the test section will need to be defined for a structure with specific area ratios. The test specimens are usually long in length to achieve the desired elastic follow-up. In the original SMT test article geometries, there is a transition region between the driver or thicker section and the test section. The transition region can be designed to represent a stress riser in a component. However, the stress and strain in this transition region and their redistribution during testing are quite complex for the SMT key feature test articles, and they are difficult, if not impossible, to measure experimentally. The stress and strain redistribution for the SMT key feature test articles was complex, and the specimens most often did not fail inside the gage section. Thus, it is difficult to directly use the test data for strain range evaluations.

In terms of testing data required for the development SMT-based design curves, it is necessary to evaluate several factors such as the elastic follow-up factor, stress concentration factor, primary load, strain range, loading rate, test temperature, and hold time. Achievement of the requisite representation of creep damage characteristics using key feature SMT, particularly at very high temperatures, involves specimen configurations that are both costly and beyond the limits of test control and stability. Although key feature SMT testing is crucial in the verification of the SMT-based design methodology, it is not practical to be used for generation of SMT-based design curves. The critical task in generating SMT-based design curves is the development of new SMT test methods to allow evaluation of the elastic follow-up effect and ensure failure inside the uniform test gage section.

In FY 2018, major progress was made in developing the two-bar SMT and single-bar SMT (SBSMT) test methods (Wang et. al, 2018, 2019). These newly developed SMT-based test methods and test protocols overcome many challenges associated with conducting SMT key feature experiments and enable the effect of elastic follow-up to be evaluated using a standard CF specimen and without the need for specialized instrumentation and specimen design. The SBSMT method can also be potentially developed into a standard test procedure. These two SMT test methods significantly simplify the procedure for generating SMT test data and enable the development of a SMT-based design approach.

In this reporting period, experiments were designed and performed on Alloy 617 and SS 316H at high temperatures in order to verify the newly developed two-bar SMT and SBSMT methods. Evaluation of the elastic follow-up effect was started with testing SS 316H at 815^{o}C using SBSMT. Test results from the pressurization SMT on Alloy 617 at intermediate strain ranges at 950^{o}C indicate that the primary load would reduce the SMT CF life. A new test confirmation was developed to allow the evaluation of the primary load effect on SMT CF life using the SBSMT technique. Additionally, selected tests were performed on SS 316H (heat 101076) to provide support for the verification of the material constitutive model developed at Argonne National Laboratory.

2. MATERIALS

The Alloy 617 specimens were machined out of the Alloy 617 plate with heat number 314626 from ThyssenKrupp VDM USA, Inc. The plate has a nominal thickness of 38 mm. The chemical composition of the plate is listed in Table 1. The specimen longitudinal direction is oriented along the rolling direction of the plate. All the specimens were tested in the as-received condition.

Table 1. Chemical compositions of Alloy 617 plate with heat number 314626 (weight %)

C	S	Cr	Ni	Mn	Si	Mo	Ti	Cu	Fe	Al	Co	B
0.05	<0.002	22.2	R54.1	0.1	0.1	8.6	0.4	0.04	1.6	1.1	11.6	<0.001

SS 316H round bar material with a nominal diameter of 25.4 mm was purchased from Outokumpu Stainless Bar, LLC. The heat number is 101076, and the as-received SS 316H bar satisfies specification per ASME SA497. The chemical composition of the SS316H is listed in Table 2. All the specimens were tested in the as-received condition.

Table 2. Chemical compositions of SS 316H bar with heat number 101076 (weight %)

C	P	Si	Ni	Mn	N	Ti	Sn	V	Fe	Cb-Ta
0.045	0.028	0.650	10.120	1.420	0.053	0.002	0.006	0.060	balance	0.014
S	**Cr**	**Co**	**Mo**	**Cb**	**Al**	**B**				
0.024	16.230	0.279	2.090	0.014	0.004	0.004				

3. PROGRESS IN PRESSURIZED SMT KEY FEATURE TESTING ON ALLOY 617

3.1 SMT KEY FEATURE TESTING WITH INTERNAL PRESSURE

The pressurized SMT experiment procedure and test configuration were explained in previous reports (Wang et al., 2014, 2015, 2016, 2018). The pressurized SMT specimen was made of three sections, with two end tabs welded to the middle tubular test section. The end tabs are to capsulate the specimen for

internal pressurization and to provide load-bearing connections with the servo-hydraulic machine for axial loading. The tubular SMT specimen and test setup are shown in Fig. 1. The test specimen has an inner diameter of 12.7 mm (0.5 in.) and a necked test section with the wall thickness of 1.524 mm (0.06 in.).

The elastic follow-up effect is caused by the stress and strain redistribution of the thicker wall tubular section and the thinner wall necked test section. The elastic follow-up factor is a function of the specimen geometry, i.e., the area ratio and the length ratio of the two sections, and the creep properties. In this case, the total effective length was controlled to be 127 mm (5 in.). The SMT method requires testing of a specimen with accurate end displacement control for the control length. Experimentally, an extensometer was adapted and extended to have a gage length of 127 mm (5 in.) with alumina rod probes in contact with the specimen surface. The 127 mm (5 in.) control length therefore includes the length of the 12.7 mm (0.5 in.) uniform necked test section, the transition length of total 2.83 mm (0.112in.) from the thicker wall section to the thin wall necked test section and a thicker section of 107.1 mm (4.217 in.), as schematically shown in Fig. 1. The tests were then performed using a strain-control mode through this 127 mm (5 in.) gage extensometer to achieve an accurate end displacement control.

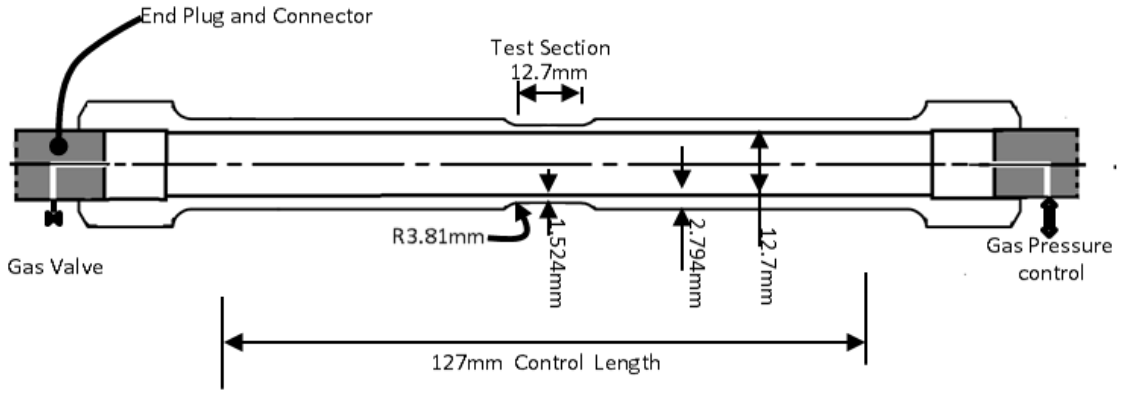

Fig. 1. Pressurization SMT specimen and experimental setup.

The end-displacement loading profile applied to the control length is schematically shown in Fig. 2. The specimen was loaded to the predefined tensile amplitude in 3 sec and held for 600 sec before unloading to the compression amplitude at the same rate. The strain ratio R was -1. The total duration for one cycle was 612 sec, and the tests were automated through a LabView program.

Although not a strict requirement for establishing design curves using the SMT-based approach, strain measurements provide insight into the role of elastic follow-up in strain redistribution. A second extensometer with a 10.16 mm (0.4 in) gage length was placed in the necked test section of the SMT specimen to measure the axial strain during the test. The stress-strain hysteresis loops were therefore obtained from these tests.

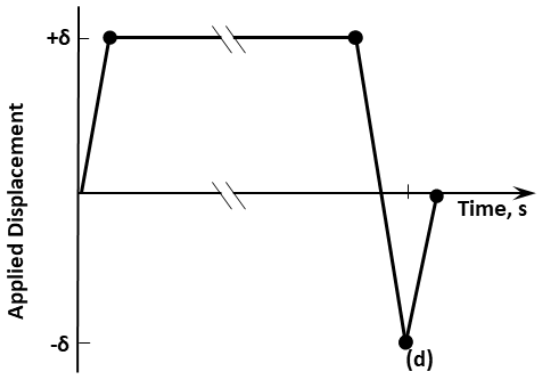

Fig. 2. Applied end-displacement profile for one cycle of SMT creep-fatigue testing with tension hold.

A three-zone resistance furnace was used to reach uniform temperature across the specimen. Multiple type S thermocouples were attached to the specimen surface using platinum wires to monitor the temperature across the control length. The maximum temperature gradient across the gage section was found to be less than 1% of the target temperature, which satisfies the ASTM E2714–09 requirement.

The tubular SMT was designed to perform SMT CF tests under constant internal pressure. It therefore combines the effects of primary load due to internal pressurization with the elastic follow-up effects configuration. The transition radius of 3.81 mm (0.15 in.) provides a stress concentration factor of about 1.45. The internal pressurization and axial loading also put the test specimen under a multi-axial stress state during testing. SMT pressurization experiments were performed at various internal pressures and amplitudes for Alloy 617 at 950^{o}C. The results are summarized below.

3.2 EFFECT OF INTERNAL PRESSURE AT LARGE STRAIN RANGE AT 950^{O}C

SMT CF tests were performed at internal pressure levels of 2 psi, 200 psi, 500 psi, and 750 psi at an amplitude of 0.114 mm (4.5 mils) at 950^{o}C with a tension hold loading profile. The 0.114 mm displacement amplitude over the 127 mm (5 in.) controlled length section corresponds to a 0.3% elastically calculated strain range in the necked test section. The results were previously discussed in detail in Wang et al. (2017). The cycles to failure are summarized here and compared in Fig. 3. The cycles to failure were the same for internal pressures of 2 psi and 200 psi but decreased from 220 cycles to 150 cycles when the internal pressure was increased from 200 psi to 750 psi. The high pressure of 750 psi decreased the SMT CF lifetime by more than 30%.

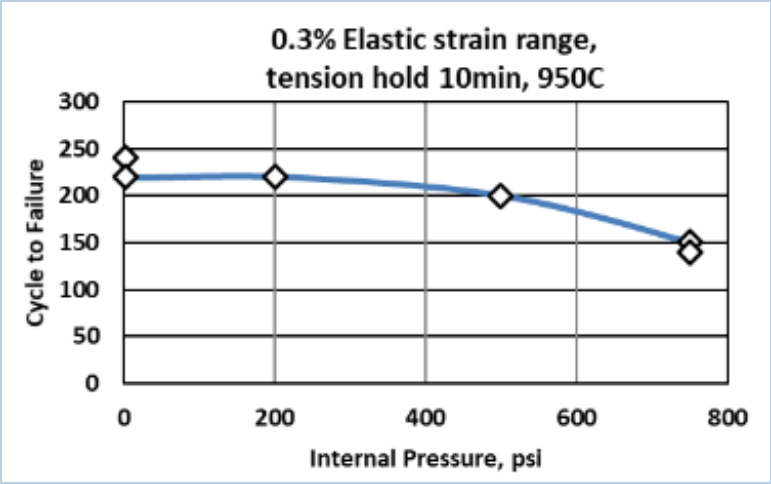

Fig. 3. Effect of internal pressure on SMT creep-fatigue at a 0.3% elastically calculated strain range with tension hold SMT creep-fatigue loading at 950°C.

In addition, all the specimens showed a noticeable amount of barreling after SMT CF with tension hold loading. The major cracks were found to be perpendicular to the axial loading direction, indicating that the axial loading was controlling the life cycles. When the internal pressure was increased to 750 psi, the failure location changed to the transition radius region, whereas the failure location was at the center of the necked test section when the internal pressure was 500 psi or lower. Two tests were repeated at 2 psi and 750 psi, and consistent results were obtained.

The results show that much higher internal pressures can reduce the number of cycles to failure. However, the internal pressure was further assessed by determining the allowable life for pressurized cylinders using the Alloy 617 allowable stress values from a proposed Code Case for Alloy 617. At 200 psi the allowable life is approximately 26,000 hr, at 500 psi it is 600 hr, and at 750 psi it is only about 80 hr. Although these initial results and analysis indicate that for normal design lives over 100,000 hr , the primary stress evaluation will screen out high-pressure loadings that would compromise cyclic life, additional testing at other strain ranges, temperatures, and hold times are required.

3.3 EFFECT OF INTERNAL PRESSURE AT INTERMEDIATE STRAIN RANGE AT 950°C

Based on the above analysis, the internal pressure for this tubular SMT geometry is limited to 150 psi for a design life of 100,000 hr at 950 °C, where the SMT creep-fatigue life cycles did not show significant changes at a large strain range. In this section, the effect of internal pressure at 2 psi and 150 psi is assessed at an intermediate strain range at 950°C with a loading amplitude of 0.0635 mm (2.5 mils) with the same loading profile shown in Fig. 2. The tension hold was kept at 600 sec. The 0.0635 mm (2.5 mils) displacement amplitude over the 127 mm (5 in.) controlled length section corresponds to a 0.17% elastically calculated strain range in the necked test section.

The hysteresis loops of the two tests for cycle #5 and cycle #100 are compared in Fig. 4. Both tests showed ratcheting to the compressive strain direction. The hysteresis loops of the test with 150 psi internal pressure showed noticeably wider hysteresis loops at cycle #100. The elastic follow-up factor at the beginning of the tests is the same for both specimens, and the value is about 4.1.

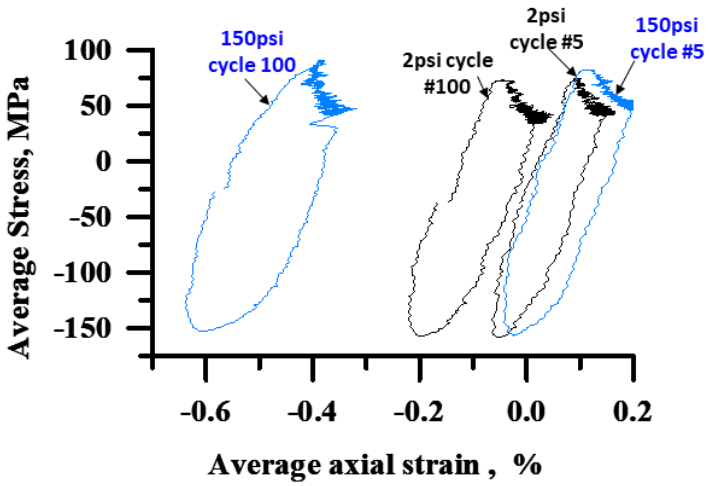

Fig. 4. Effect of the internal pressure on hysteresis loops.

Comparison of the maximum and minimum stresses, the maximum and minimum strains, and strain ranges in the necked test section are plotted in Fig. 5. The test with 150 psi failed at 870 cycles, which is 66% of the SMT life cycles of the test with an internal pressure of 2 psi with 1300 cycles (the cycles for failure initiation are used as the failed cycle here). The tests with 150 psi internal pressure showed much a faster ratcheting rate as a function of applied cycles.

The results suggest that the higher internal pressure reduced the SMT CF life even though the internal pressure was within the allowable value for a 100,000 hr design life limit. It is noted that the number of tests is limited. Additional future tests under the same test conditions would help to assess the data scatter. However, the results in this study indicate that the impact of primary load on SMT CF life is worthy of further investigation.

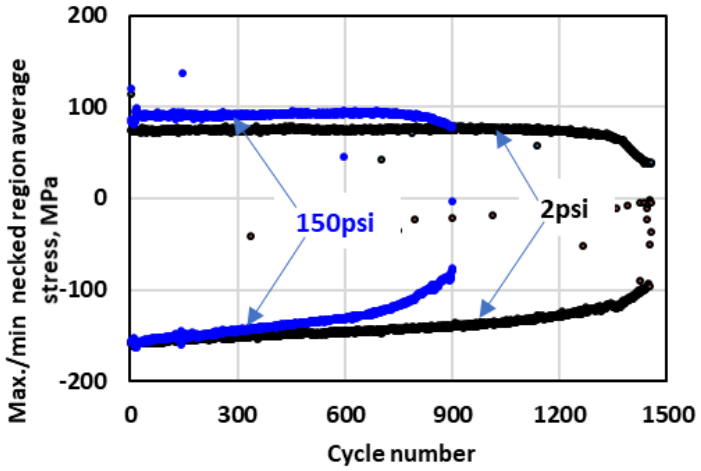

(a)

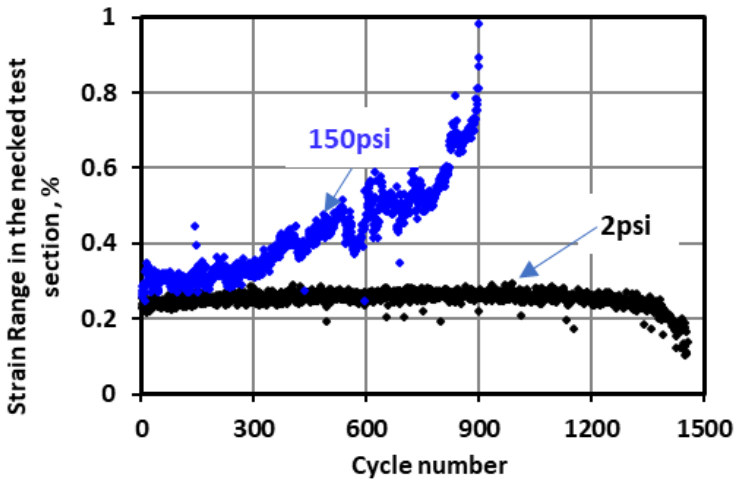

(b)

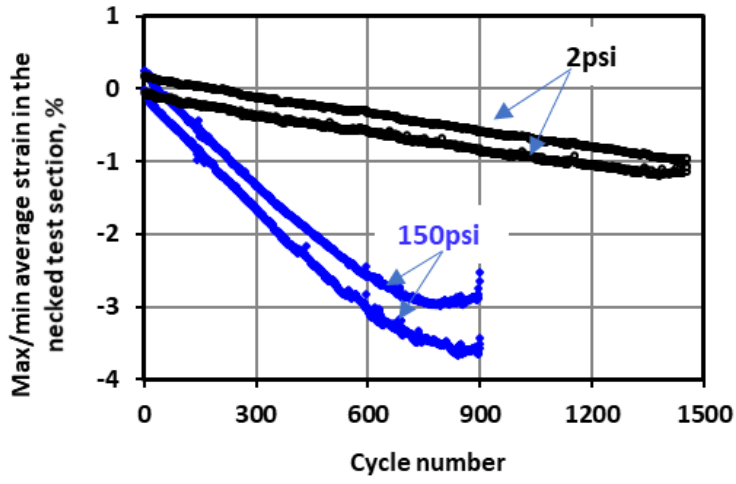

(c)

Fig. 5. Comparison of the maximum and minimum stresses (a), strain ranges (b), and maximum and minimum strains (c) as a function of cycles for pressurized SMT at 950°C.

Photos of the failed specimens are shown in Fig. 6. Both specimens showed a significant amount of barreling. The outside diameter (OD) at the center of the necked test section of the test with 2 psi internal pressure increased from 15.75 mm (0.62 in.) to 16.26 mm (0.64 in.), whereas the test specimen with 150 psi internal pressure showed an OD of 17.02 mm (0.67 in.) after failure. The extent of barreling for these two specimens is consistent with the degree of ratcheting.

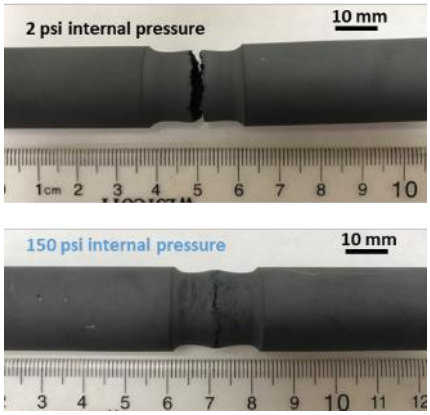

Fig. 6. Photos of the failed specimens tested at 950ºC.

3.4 EFFECT OF INTERNAL PRESSURE AT INTERMEDIATE STRAIN RANGE AT 850ºC

At a high temperature of 950ºC, stress relaxation is significant for Alloy 617 for a hold time of 600 sec. To have a complete picture of the primary load effect on the SMT CF life, additional tests at lower temperatures are needed. Based on the above test and analysis at 950ºC, when the internal pressure for this tubular SMT geometry is limited to the stress allowable for a design life of 100,000 hr, the results show that the SMT life was not affected by the internal pressure at a larger strain range, but SMT CF life decreased when tested for longer durations at intermediate strain ranges. In this section, the effect of internal pressure at intermediate strain ranges is assessed at a lower temperature of 850ºC. At this temperature, the internal pressure limit calculated from the stress allowable for a design life of 100,000 hr is 400 psi. To evaluate the effect of internal pressure, two pressurized SMT were performed at 850ºC, with one at an internal pressure limit of 400 psi and the second test at 2 psi. The loading amplitude was 0.0762 mm (3 mils), and the same loading profile shown in Fig. 2 was applied.

The strain ranges and maximum and minimum strains measured at the necked test section are shown in Fig. 7. The initial stable strain ranges were similar, with 0.21% for the test with an internal pressure of 400 psi and 0.25% for the test with an internal pressure of 2 psi. Both specimens showed ratcheting to the compressive strain direction, and the total ratcheting strain was more than 1%. The ratcheting rates were faster initially but slowed down upon reaching a steady state after about 500 applied cycles. The difference in the ratcheting rate at steady state was insignificant for the two tests.

The maximum and minimum stresses are compared in Fig. 8. Both tests showed similar maximum and minimum stress levels and cycles to failure of 3350. Photos of the failed specimens are shown in Fig. 9. Both specimens showed slight barreling at the necked test section, and the major cracks were located at the middle of the necked section as well as at the root of the transition region between driver and necked test section.

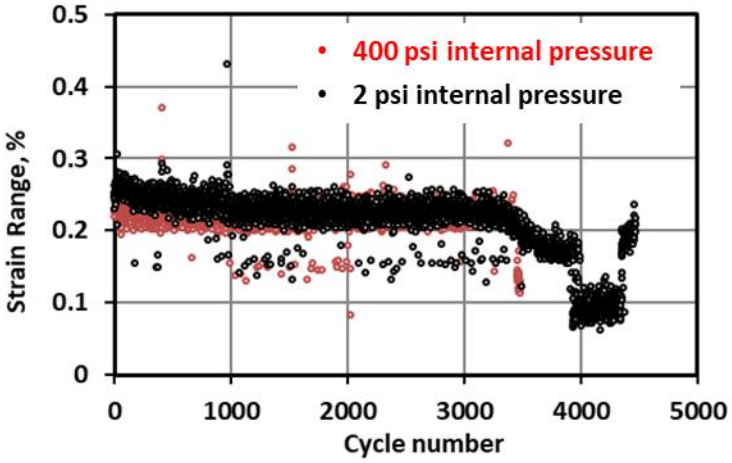

(a)

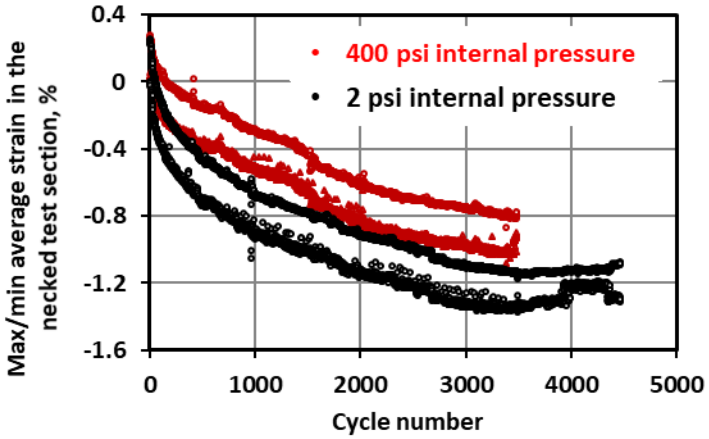

(b)

Fig. 7. Comparison of the strain ranges (a) and the maximum and minimum strains (b) for pressurized SMT at 850°C.

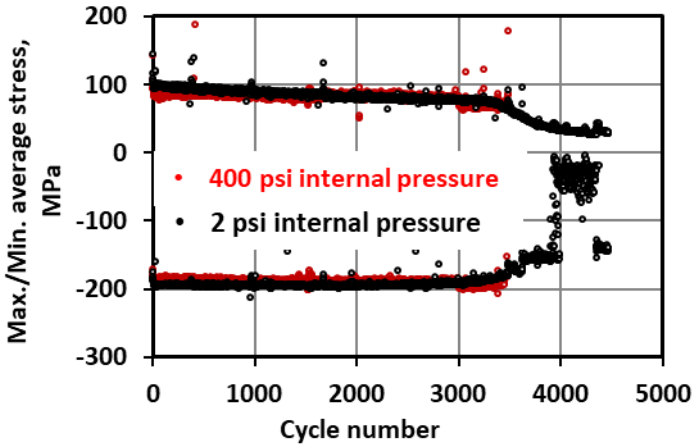

Fig. 8. Comparison of the maximum and minimum stresses as a function of cycles for pressurized SMT 850°C.

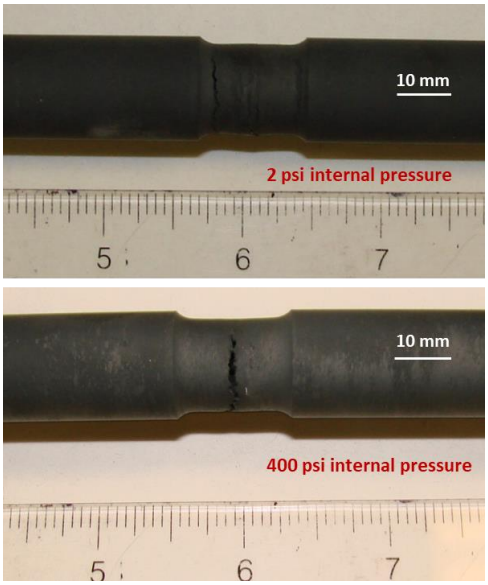

Fig. 9. Photos of the failed specimens tested at 850°C.

3.5 SUMMARY OF PRESSURIZED SMT TEST RESULTS

All the SMT tests performed on Alloy 617 at 950°C and 850°C with internal pressurization and tension hold loading are summarized in Table 3. The tests discussed above that were completed during this reporting period are highlighted. At a large strain range and high temperature of 950°C, the effect of allowed internal pressure determined by the primary load allowable on the SMT CF life is insignificant. However, based on limited test data at an intermediate strain range of ~0.25%, SMT CF life decreased due to the internal pressure, although it was within the allowable limit for a 100,000 hr design life at 950°C. When the test temperature was decreased to 850°C, the SMT CF life was not affected by the allowable internal pressure limit of 400 psi for a 100,000 hr designed life.

The effect of primary load on SMT design curve is an important aspect of the SMT-based design methodology. Additional SMT tests with internal pressurization at different strain ranges, temperatures, and hold times are certainly needed to understand the data scatter and fully evaluate the effect of primary load on the SMT CF life. The limited test data listed in Table 3 indicate that the effect of primary load is dependent on test temperature and strain ranges. Additionally, numerical or analytical analysis on the EPP strain range of SMT tests with internal pressure would shed light on how to consider the primary load in the integrated EPP plus SMT design approach.

Table 3. Results of pressurized SMT for Alloy 617 with tension hold

Specimen ID	Amplitude, δ value	Initial strain range	Test temperature (°C)	Internal pressure	Lifetime (hr)	Cycles to failure
INC617-P01	0.114 mm (or 4.5 mils)	0.8%	950	0.01MPa (or 2 psi)	37.4	220
INC617-P02		0.8%	959	1.38MPa (or 200 psi)	37.4	220
INC617-P04		0.8%	957	3.45MPa (or 500 psi)	34	200
INC617-P03		0.75%	958	5.17MPa (or 750 psi)	25.5	150
INC617-P06		0.8%	950		23.8	140
INC617-P09	0.076 mm (or 3 mils)	---	953		54.4	320
INC617-P10	0.025 mm (or 1 mils)	0.12%	950	1.03MPa (or 150psi)	>6408	>37,693
INC617-P11*	0.0635 mm (or 2.5 mils)	0.4%	950	1.05MPa (or 150 psi)	18.7	110
INC617-P12		0.25%	950	0.01MPa (or 2 psi)	231.2	1360
INC617-P13		0.25%	950	1.05MPa (or 150 psi)	139.4	820
INC617-P14	0.0762 mm (or 3 mils)	0.21%	850	2.76MPa (or 400 psi)	584.2	3440
INC617-P15		0.25%	850	0.01MPa (or 20 psi)	584.8	3460

Note: * INC617-P11 is for information only. The initial large strain range indicates a specimen with possible defects.

4. PROGRESS IN TWO-BAR SMT AND SINGLE-BAR SMT TESTING

4.1 SPECIMEN AND SMT CREEP-FATIGUE LOADING PROFILE

Experiments were designed for Alloy 617 and SS 316H using the SBSMT test method. The specimen geometry is shown in Fig. 10. It is a standard CF specimen with a gage diameter of 6.35 mm and a uniform gage length of 19.05 mm.

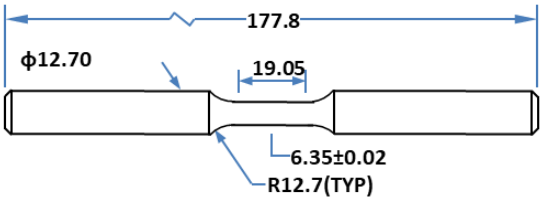

Fig. 10. Geometry of the standard creep-fatigue specimen (units are in mm).

The SBSMT CF used a trapezoid loading profile, as shown in Fig. 2. The holding time was applied at the maximum tension. The loading was fully reversed with strain loading ratio of R = -1.

4.2 SMT CREEP-FATIGUE EVALUATION ON ALLOY 617

Two SMT tests were designed and performed at 950°C on Alloy 617: two-bar SMT with a driver at 950°C (i.e., hot driver two-bar SMT) and single smooth bar SMT (or SBSMT). These two tests had the same elastic factor of about 3.1, as what was previously tested using two-bar SMT with a room temperature driver (i.e., cold driver two-bar SMT) described by Wang et al. (2018). The purpose of these tests was to verify the new SMT test methods established in FY 2018. The elastically calculated strain range was 0.3% for the tests. The specimens were loaded with a tension hold time of 600 s and fully reversed strain

amplitude, as shown in Fig. 2. The loading time to maximum tension amplitude was 3 s, corresponding to a strain rate of approximately 1.3E-3/s.

The hysteresis loops for cycle #30 and #400 are compared in Fig. 11. Cycle #400 is about the mid-life cycle for the three tests. For easier comparison, the ratcheting strain in the hot driver two-bar SMT test was removed. The relaxation slopes of the cold driver two-bar SMT and the single smooth bar SMT are nearly identical, both of which showed an elastic follow-up factor of 3.1 as designed. The elastic follow-up factor of the hot driver two-bar SMT was 2.8, slightly lower than the designed value of 3.1. This decrease was attributed to the creep behavior of the hot driver, which lowered the effectiveness of its spring constant. For all three cases, the elastic follow-up factor did not show any noticeable changes as a result of an increase in the number of cycles.

The three specimens were tested to failure with the failure location inside the uniform gage section. The maximum and minimum stresses, the strain ranges, and the maximum and minimum strains measured as a function of test cycles are compared in Fig. 12. The maximum and minimum stresses are comparable, and the initial stable strain ranges are similar for the three tests. The strain range increased as the number of CF cycles increased. The maximum and minimum strains measured as a function of cycles showed the same trend for the cold driver two-bar SMT and SBSMT. However, although the strain ranges were similar to the other two tests, the hot driver SMT experienced compressive ratcheting strain. The total ratcheting strain was about -3% before failure. This compressive ratcheting behavior was also observed in the original key feature SMT under similar test conditions. The ratcheting behavior was caused by the slightly creeping behavior of the hot driver bar during the test.

The cycles to failure initiation were similar for the three tests, with 825 cycles for the hot driver two-bar SMT, 875 cycles for the cold driver two-bar SMT, and 855 cycles for the single smooth bar SMT.

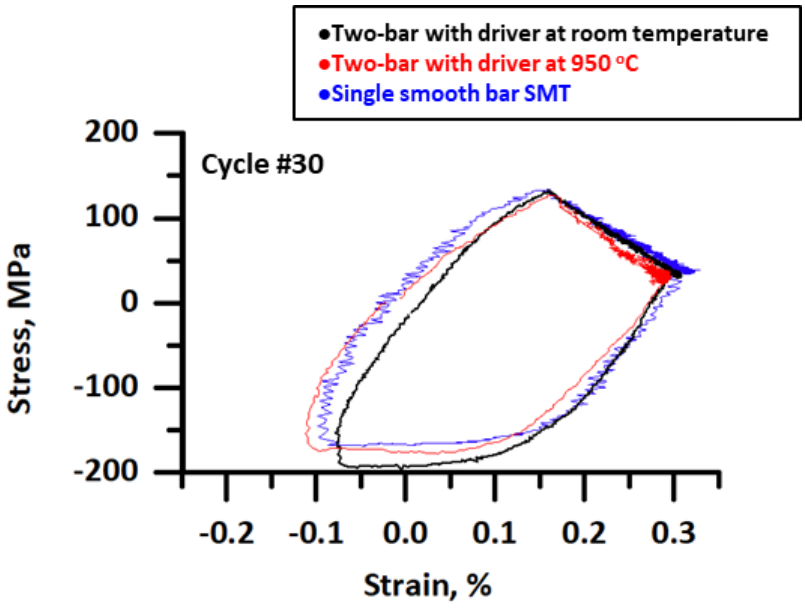

(a)

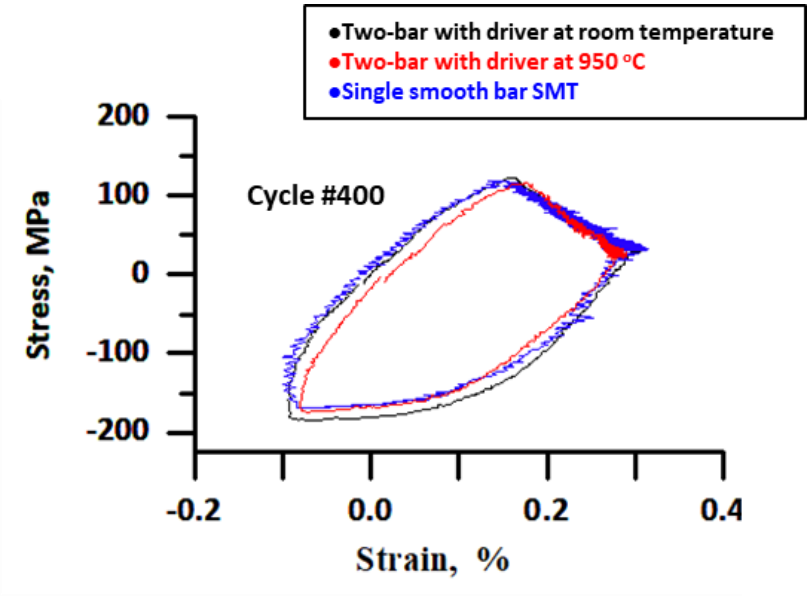

(b)

Fig. 11. Comparison of the hysteresis loops for cycle #30 (a) and cycle #400 (b) of the two-bar SMT tests and SBSMT on Alloy 617 at 950°C.

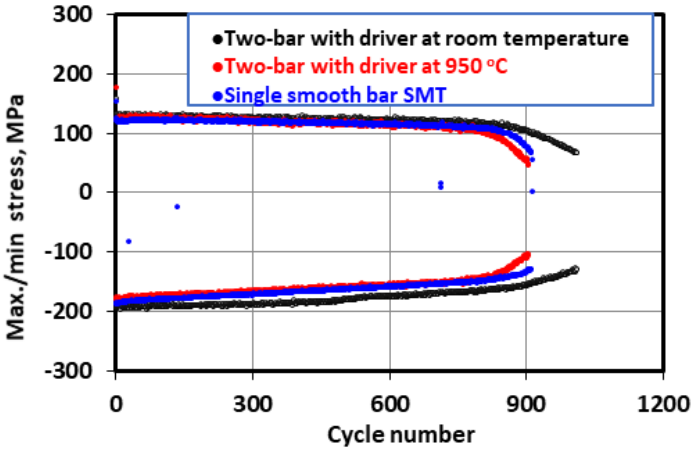

(a)

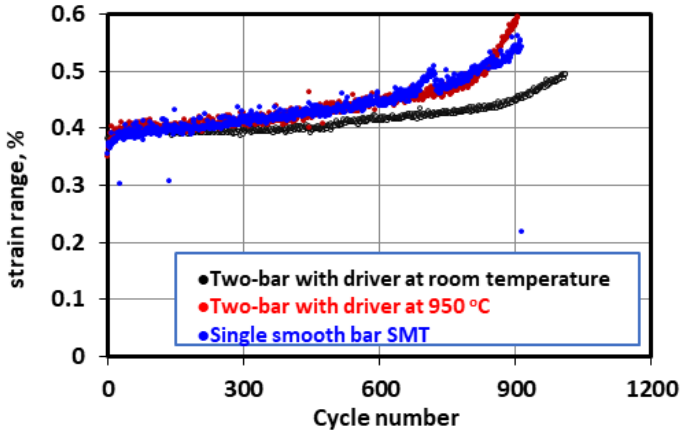

(b)

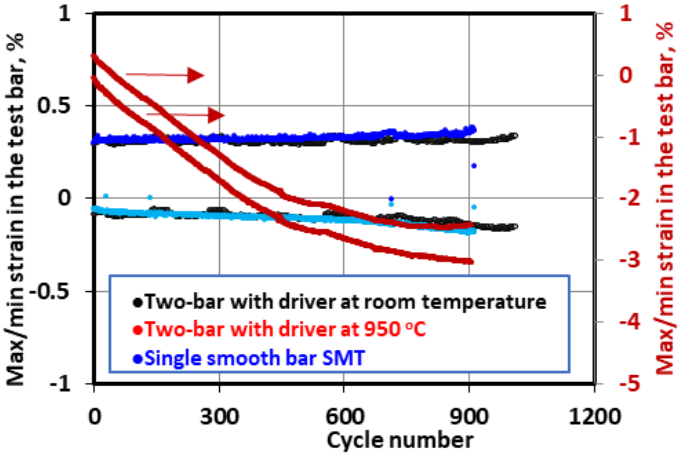

(c)

Fig. 12. Maximum and minimum stresses (a), strain ranges (b), and the maximum and minimum strains (c) of the two-bar SMT and SBSMT on Alloy 617 at 950ºC.

4.3 TWO-BAR SMT CREEP-FATIGUE EVALUATION ON SS 316H

Two SMT tests were designed and performed at 815°C on SS 316H: two-bar SMT with a driver at 815°C (i.e., hot driver two-bar SMT) and two-bar SMT with a room temperature driver (i.e., cold driver two-bar SMT). These two tests were designed to have the same elastic factor of about 3.4. The purpose of these tests was to further verify the new SMT test methods and to check the dependence of the testing methods on testing materials. The principle of the two-bar SMT design concept uses the ratio of the spring constant of the driver and the test bar to determine the elastic follow-up factor (Wang et al., 2018, 2019); it therefore should be independent of the type of testing material provided the proper elastic spring constants are used in the test design.

For these two-bar SMT experiments, the elastically calculated strain range was 0.3%, and the initial stable strain range was 0.45%. The specimens were loaded with a tension hold time of 600 s and fully reversed strain amplitude, as shown in Fig. 2. The loading time to maximum tension amplitude was 3 s, corresponding to a strain rate of approximately 1.5E-3/s.

The hysteresis loops and the stress relaxation curves for cycle #30 and half life cycle #600 are compared in Fig. 13 and Fig. 14. For easier comparison, the ratcheting strain in the hot driver two-bar SMT test was removed. The elastic follow-up factor calculated from the relaxation slope was 3.4 for the cold driver SMT, whereas the hot driver two-bar SMT showed a slightly lower elastic follow-up value of 3.0. The cold driver SMT with higher elastic follow-up showed slower stress relaxation behavior. The lower elastic follow-up for hot driver two-bar test was also observed for Alloy 617, and it is likely due to the creep of the hot driver in the two-bar SMT test configuration. For both cases, the elastic follow-up factor did not show any noticeable changes as a result of an increase in the number of applied cycles.

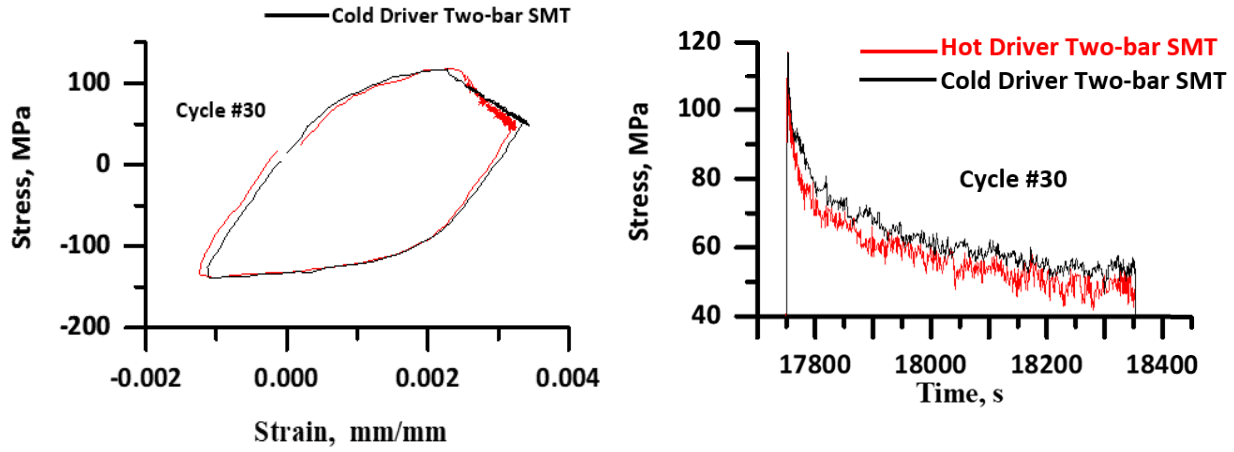

(a) (b)

Fig. 13. Comparison of the hysteresis loops (a) and stress relaxation curves (b) for cycle #30 of the two-bar SMT on SS 316H at 815°C.

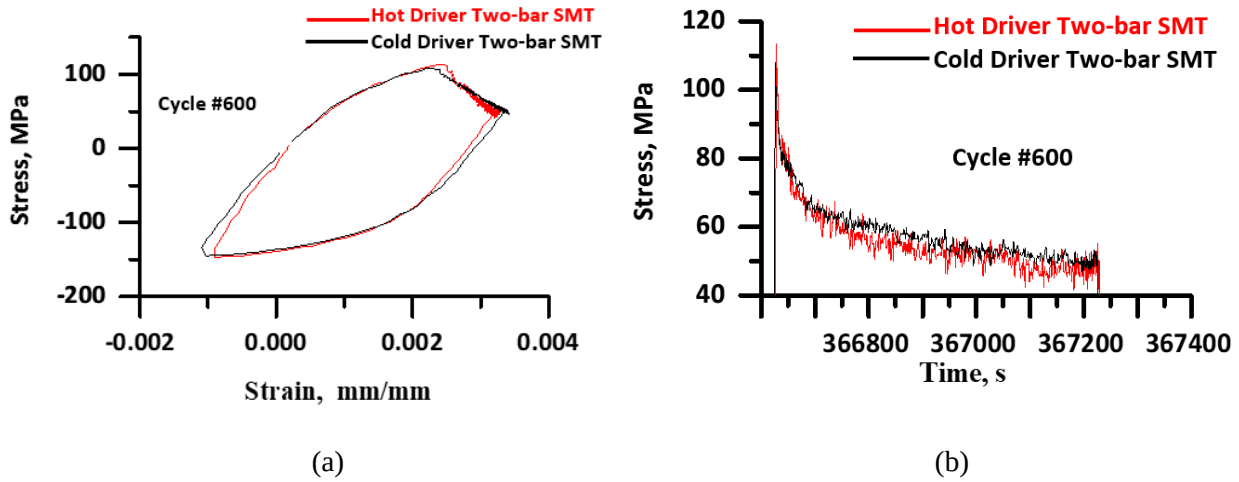

Fig. 14. Comparison of the hysteresis loops (a) and stress relaxation curves (b) for cycle #600 of the two-bar SMT on SS 316H at 815ºC.

Both specimens were tested to failure with the failure location inside the uniform gage section, as shown in Fig. 15. The maximum and minimum stresses, the strain ranges, and the maximum and minimum strains measured as a function of test cycles are compared in Fig. 16. The maximum and minimum stresses were similar, and the initial stable strain ranges were both approximately 0.45%. The strain range significantly increased as a function of applied cycles failure initiation. The hot driver SMT specimen experienced compressive ratcheting strain, similarly to what was observed with Alloy 617. The total ratcheting strain was about -2% before failure. This compressive ratcheting behavior was also observed in the original key feature SMT for SS 316H under similar test conditions. The ratcheting behavior is caused by the slightly creeping behavior of the hot driver bar during the test.

The cycles to failure initiation were 1000 for the hot driver two-bar SMT test and 1200 for the cold driver two-bar SMT.

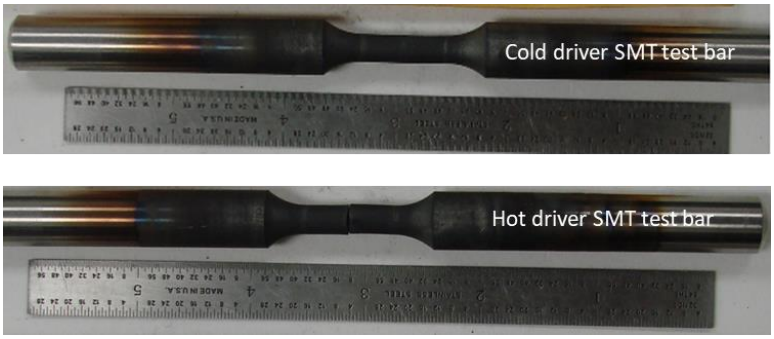

Fig. 15. Photos of the failed SS 316H specimens after two-bar SMT at 815ºC.

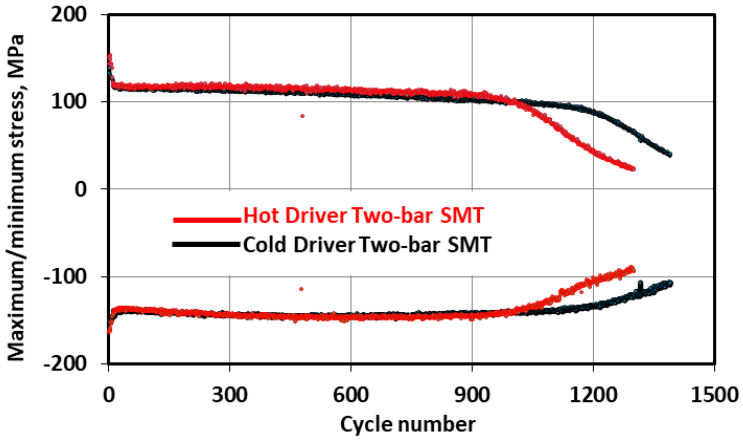

(a)

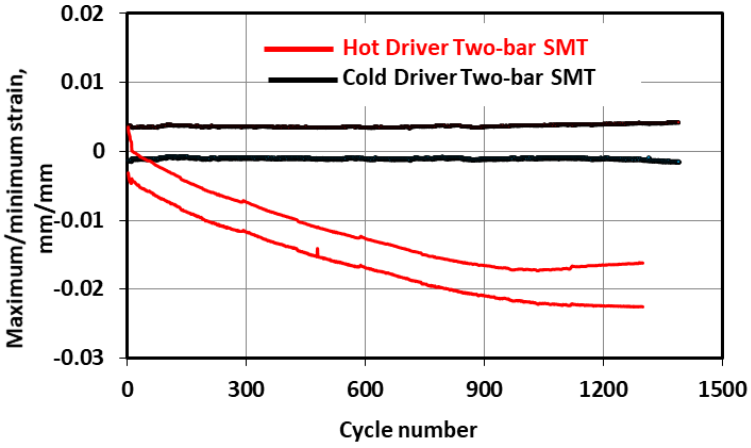

(b)

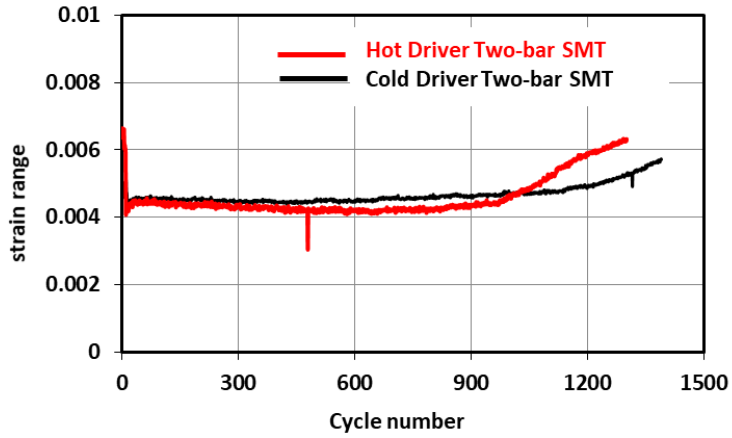

(c)

Fig. 16. Maximum and minimum stresses (a), maximum and minimum strains (b), and strain ranges (c) of the two-bar SMT on SS 316H at 815ºC.

4.4 EVALUATION OF THE ELASTIC FOLLOW-UP EFFECT ON SS 316H USING SBSMT

Compared with the two-bar SMT and the original SMT test methods, the SBSMT test method is the preferred technique used to evaluate the elastic follow-up effect on the SMT CF life. The reason is that SBSMT significantly reduces the complexity of the testing configuration and test specimen geometry by performing SMT-based evaluations similar to those of the standard CF and using standard CF specimens. In this section, experiments were designed for SS 316H (heat 101076) with three different elastic follow-up factors to assess its effect on SMT CF life.

The three SBSMT tests on SS 316H were conducted at 815°C. The initial stable total strain range was 1% with a nominal strain rate of 1E-3 mm/mm/s using standard CF specimen, as shown in Fig. 10. The tension hold segment was 600 s. The hysteresis loops and stress history of cycle #50 for the three tests are compared in Fig. 17. For easier comparison, the hysteresis loops of the Q=6 and Q=12 were offset in the strain axial to overlay on top of the standard CF. Cycle #50 was a stabilized cycle in the three tests and can represent the typical characteristics of each tests. As clearly shown, the higher the elastic follow-up, the slower the stress relaxation during holding.

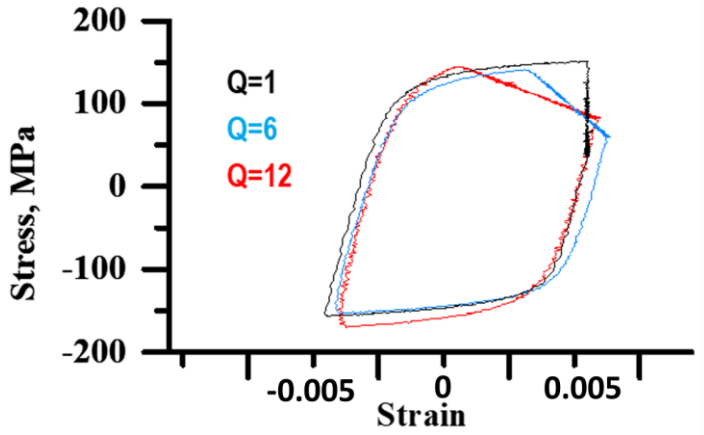

(a)

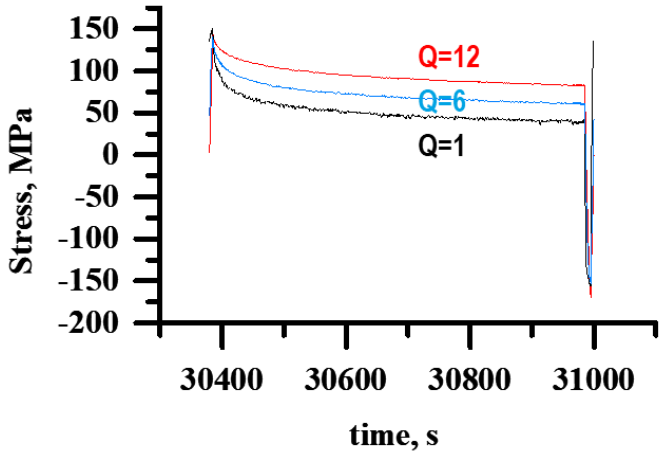

(b)

Fig. 17. Elastic follow-up effect on hysteresis loops (a) and stress histories (b) of cycle # 50 for SS 316H tested at 815°C using SBSMT.

To quantitively describe the elastic follow-up effect, the features of the hysteresis loop with elastic follow-up are schematically defined in Fig. 18, and the corresponding values of each parameter are listed in Table 4. The elastic follow-up effect caused a 0.524% relaxation strain for Q=12 and 0.321% for Q=6. For standard CF testing with Q=1, there is no change in relaxation strain during holding. To achieve the same total strain of about 1%, the specimen with Q=12 was only loaded with an elastically calculated strain range of 0.486. That is, elastic follow-up with Q=12 increased the creep strain in the specimen by a factor of 2. More importantly, the stress relaxed only 41.9% at end of the holding segment for Q=12, but 73.6% for the standard CF with Q=1. The higher stress during the holding segment causes more creep damage.

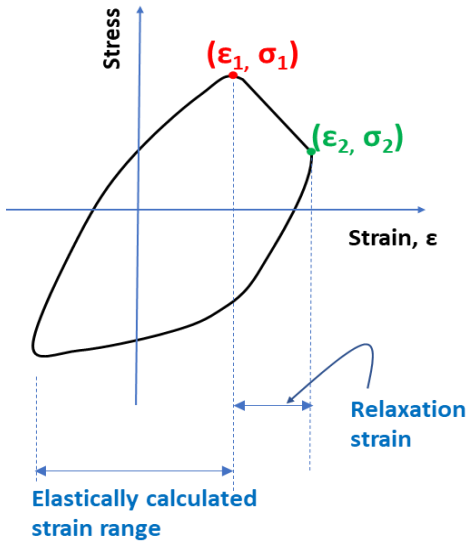

Fig. 18. Characteristics of the hysteresis loop of the SBSMT test.

Table 4. Comparison of SBSMT cycle #50 for SS 316H (Heat No. 101076)

Elastic follow-up factor	Total strain range	Elastically calculated strain range	Relaxation strain (ε_2-ε_1)	Relaxed stress level and end of holding, σ_2 (MPa)	Percentage of the stress relaxation (1-σ_2/ σ_1)
Q=1	1.026%	1.026%	0	39.4	73.6%
Q=6	1.057%	0.737%	0.321%	60.6	56.6%
Q=12	1.010%	0.486%	0.524%	83.9	41.9%

Additional representative hysteresis loops for the three tests are compared in Fig. 19. The characteristics of the hysteresis loops did not show any noticeably changes in the stable state, and the elastic follow-up factor remained the same.

The maximum and minimum stresses and the strain ranges as a function of applied cycles for the three tests are shown in Fig. 20. The cycles to failure were 180 for the test with Q=12, slightly lower than the 200 cycles to failure for both Q=1 and Q=6.

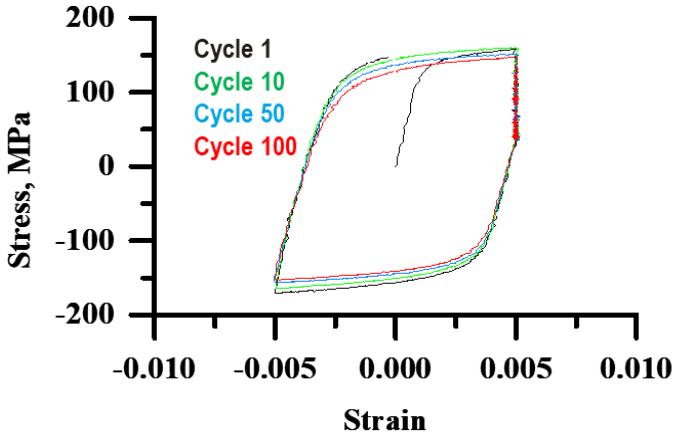

(a)

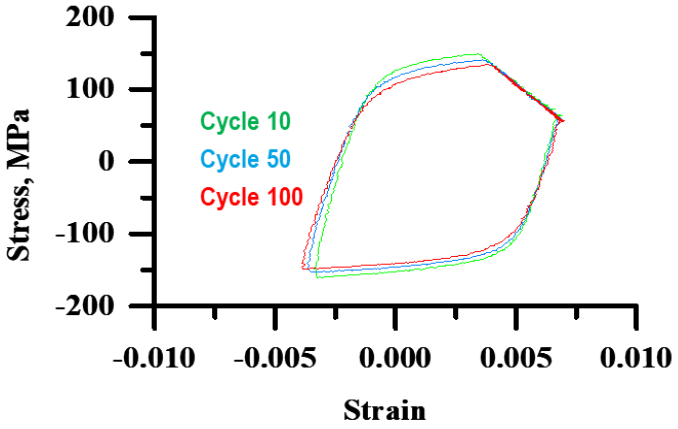

(b)

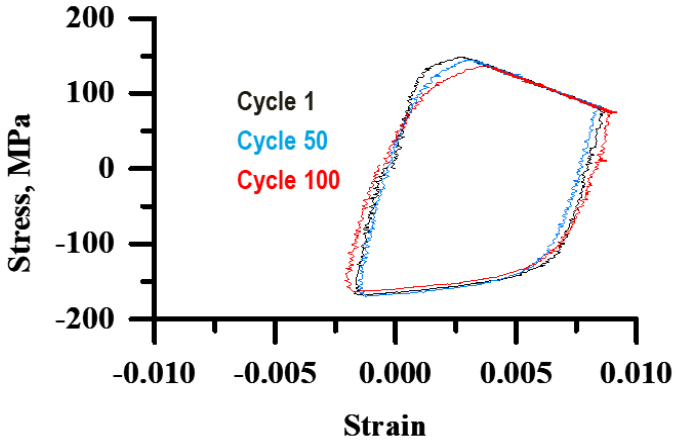

(c)

Fig. 19. Comparison of hysteresis loops of the SBSMT with elastic follow-up factor of Q=1 (a), Q=6 (b), and Q=12 (c) on SS 316H at 815ºC.

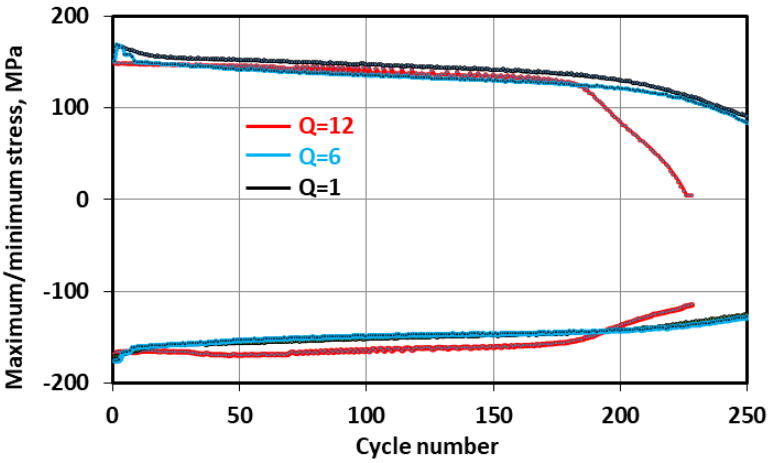

(a)

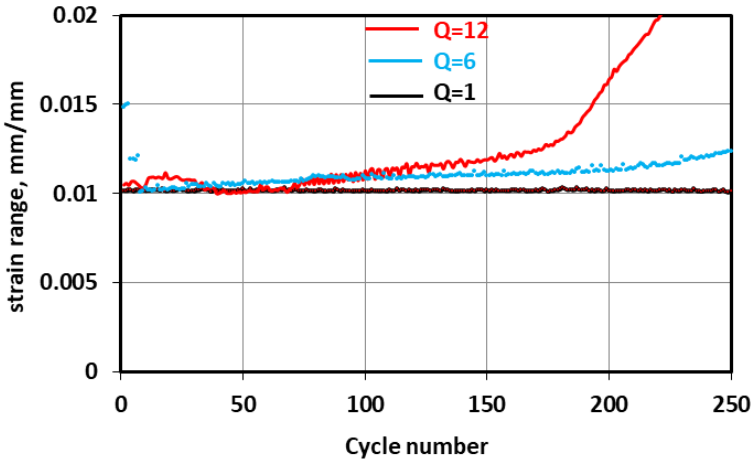

(b)

Fig. 20. Maximum and minimum stresses (a) and strain ranges (b) of the SBSMT on SS 316H at 815ºC.

4.5 SBSMT SPECIMEN DESIGN WITH INTERNAL PRESSURIZATION

In the original SMT design method development plan, pressurized tubular SMT key feature specimens were used to evaluate the effect of primary load on SMT CF life. As discussed and demonstrated in Section 3, the test configuration of the original pressurized SMT is highly specialized and the test results are often difficult to interpret due to the complex stress and strain redistribution between the driver section, the transition region, and the necked test section. Additionally, the cost of machining and assembling the large tubular SMT specimen was high, which made it impractical to perform a large number of tests with internal pressurization. This became a major disadvantage in the development of the SMT design methodology.

To take advantage of the newly developed SBSMT method, a tubular specimen configuration was designed. The tubular geometry allows internal pressurization, and the SBSMT provides a much more

compact specimen design. A drawing of the specimen is shown in Fig. 21. The wall thickness, internal diameter, and surface finish requirement of the gage section of the pressurized SBSMT specimen are the same as the necked test section of the original tubular SMT specimen shown in Fig. 1. By using the pressurized SBSMT method, evaluation of the primary load effect on SMT CF life is expected to be much easier and simpler. The complex issues of ratcheting and barreling in the original pressurized SMT are expected to be resolved or minimized by the SBSMT method.

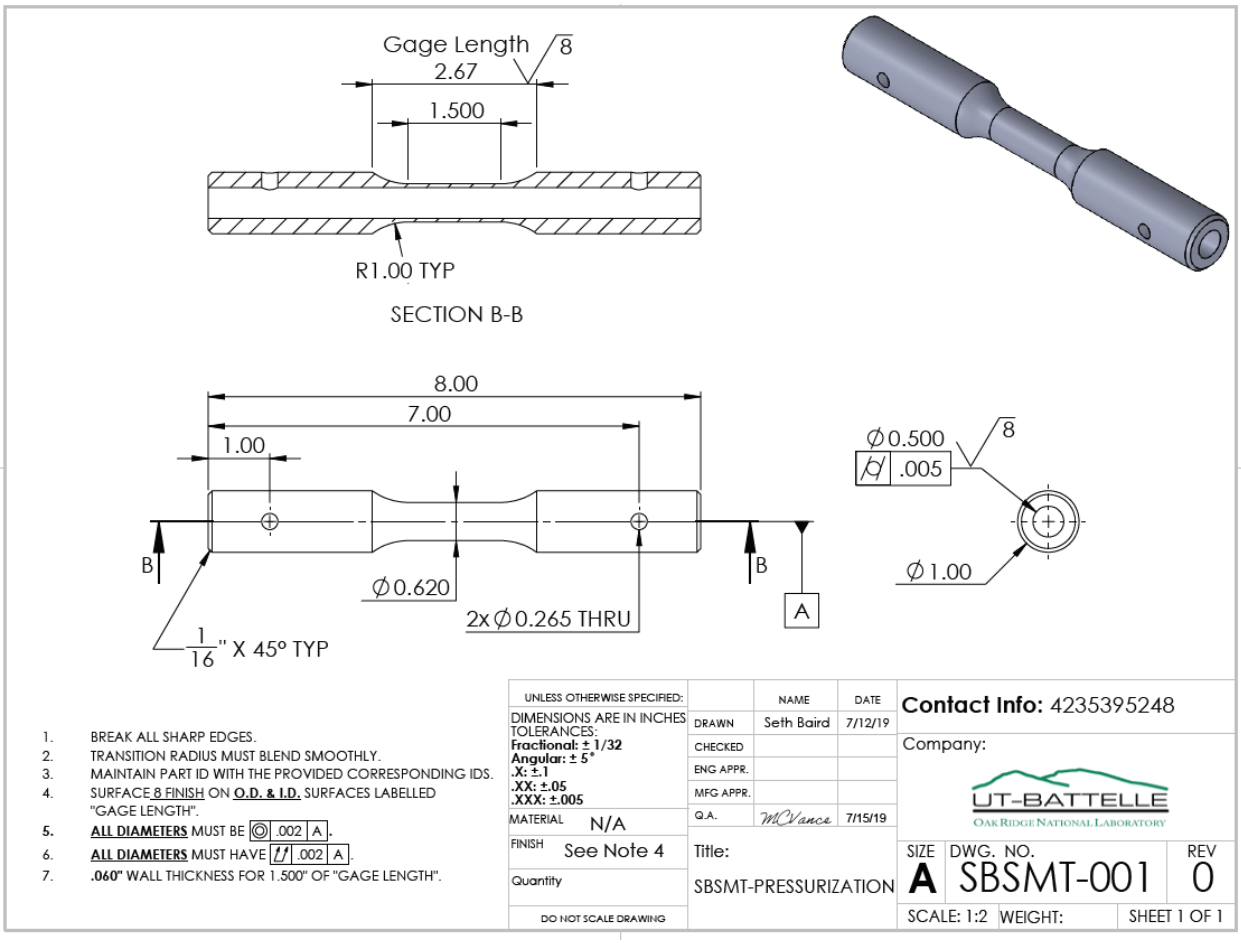

Fig. 21. Specimen geometry of pressurized SBSMT (units are in inches).

4.6 DISCUSSION OF THE TWO-BAR SMT AND SBSMT RESULTS

In the original SMT key feature testing methods, the elastic follow-up factor was achieved by sizing the length and area ratio of the driver section to the test section. In some cases, with large elastic follow-up, testing becomes impractical due to the buckling of long specimens. In addition, the precise end displacement control becomes critical due to the increased extensometer span. One of the key features of the original SMT test articles is the designed stress concentration factor at the transition radius between the two section. However, the transition region was often the failure location, causing the analysis to become more complex due to the unknown stress and strain quantities. In reviewing the original SMT key feature testing results in support of the development of a new CF design approach, the complex material responses to SMT key feature testing imposed major difficulties in extracting information from these tests

to verify the analysis. The two-bar SMT method has effectively resolved these critical challenges. The two bars are individual standard uniaxial CF specimens, and the stress and strain are directly measured. The two-bar SMT with a driver at the same test temperature represents the response of the high-temperature component under elastic follow-up effect but without the localized deformation, which greatly simplifies testing and evaluation of the elastic follow-up effect.

Two-bar SMT with an elastic driver bar is the same as the single smooth bar SMT in theory, as confirmed by the test results for Alloy 617 above. The test setup and procedure for the single smooth bar SMT is much simpler and similar to the standard CF test described in ASTM E2714. The major difference is the addition of the electronic component for generating the equivalent strain signal from the measured load and then combining it with the strain from the test specimen to form the control strain signal. However, these features can be implemented relatively easily in most of modern test controllers. This single smooth bar SMT method therefore has the potential to become a standard test method and be used by a broader research community.

The two-bar SMT with a driver at the same high temperature as the test bar showed a slightly lower elastic follow-up factor than designed. This is because the driver bar at high temperature is not perfectly elastic as compared with the ideal elastic assumption. The driver bar experienced mild creeping under the loading conditions, resulting in the observed ratcheting strain in the test bar in addition to a slightly lower elastic follow-up. However, the SMT CF life was not affected by the slightly different elastic follow-up factor and the ratcheting strain for both Alloy 617 and SS 316H. In the design process for a component, there would be limited ratcheting with the deformation limits evaluation. The effect of ratcheting strain in the SMT CF experiments was thus determined to be an insignificant factor for SMT-based design.

The two-bar SMT and SBSMT methods capture the essential features of a test article with elastic follow-up, i.e., the retarded stress relaxation and the enhanced creep fatigue damage shown from the enlarged strain ranges. These two effects are built into the SMT test data. A key point in the SMT-based design approach is that separate evaluation of creep and fatigue damage is no longer required. The enhanced creep damage due to elastic follow-up is accounted for in the SMT test data. The development of the new SMT testing methods allowed major progress to be made in generating SMT-based design curves to assess the cyclic damage in the component at high temperatures. Additionally, the new concept of using pressurized SBSMT to evaluate the primary load effect has greatly simplified the testing program.

To generate SMT-based design curves, several parameters will need to be considered in the test program. The first is the selection of a bounding or representative elastic follow-up factor for most high-temperature components. Accomplishing this will require numerical and analytical analysis of the elastic follow-up responses of representative key featured components. This process ensures the design of SMT experiments with reasonable elastic follow-up magnitude without excessive conservatism. Another important parameter is the hold time effect since design lives will be much greater than the test duration. Methodologies for extrapolating hold time effects will be required. Such extrapolation will be greatly simplified if it can be demonstrated that degradation of cyclic life with hold time saturates and that there is essentially no further degradation as the hold time increases. Strain rate effect will also need to be considered in the test program. A design margin must be applied to the test data to account for factors such as data scatter, extrapolation to longer hold times, etc.

5. HIGH-TEMERPATURE MECHANICAL CHARATERIZATION OF SS 316H WITH HEAT NO. 101076

The SS 316H bar stock with heat number of 101076 was purchased by the ART program to support the development of the integrated EPP plus SMT design method and to verify the material constitutive model developed at ANL. As explained in Section **Error! Reference source not found.**, SS 316H satisfies A

SME SA497. The heat of SS 316H also meets the additional restrictions of 0.05% minimum nitrogen, 0.03% maximum aluminum, and 0.04% maximum titanium for service temperatures higher than 1100°F (595°C). However, the high-temperature mechanical behavior for this particular heat of SS 316H is not available. In FY 2019, selected standard uniaxial mechanical tests were performed because of the lack of information on SS 316H (heat 101076).

ASME SEC III Div.5 HBB-2800-FATIGUE ACCEPTANCE TEST, Paragraph (b) stated the following:

> *The fatigue test shall be performed in air at 1,100°F (595°C) at an axial strain range of 1.0% with a 1-hr hold period at the maximum positive strain point in each cycle. Test-specimen location and orientation shall be in accordance with the general guidance of SA-370, paras. 6.1.1 and 6.1.2 and the applicable product specifications. Testing shall be conducted in accordance with ASTM Standard E 606. The test shall exceed 200 cycles without fracture or a 20% drop in the load range*.

This testing procedure was followed, and the maximum and minimum stresses are plotted in Fig. 22. The number of cycles to failure was 440, which is more than twice that of the required 200 cycles. This confirms that SS 316H can be accepted for use in Class A elevated temperature components.

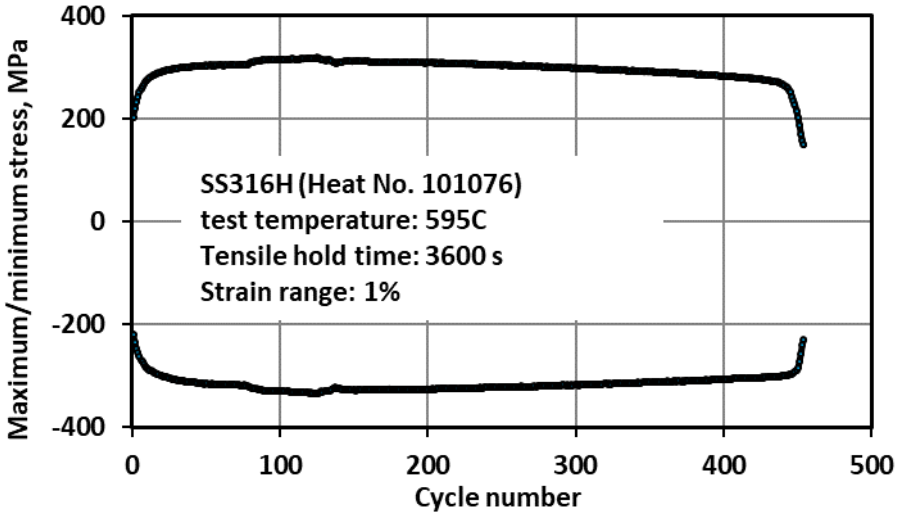

Fig. 22. Fatigue acceptance test on SS 316H (heat 101076) at 595°C.

Standard tensile testing was performed at 815°C following ASTM E21 standard. The stress-vs-strain curve is shown in Fig. 23. The yield strength and ultimate tensile strength were 137.5 MPa and 187.6 MPa, respectively.

Standard strain-controlled CF tests were performed at 815°C per ASTM E 606 at strain ranges of 0.5% and 1%. The maximum and minimum stresses as a function of applied cycles are plotted in Fig. 24 and Fig. 25. The cycles to failure for 0.5% strain range with 600 s tensile hold were 828 and for 1% strain range with both 600 s and 1800 s (0.5 hr) tensile hold tests were 220 cycles.

It is interesting that the cycles to failure were not affected by the hold time at 1% at 815°C. Plots of the stress histories and the hysteresis loops of the initial cycles are shown in Fig. 26. The hold time of 600 s was not long enough to reach a saturated stress state. There are no significant differences in the shape of

the hysteresis loops of similar cycles for both tests. The results indicate that the creep damage due to the accumulated higher stresses during the 600 s hold time is equivalent to the longer time at lower stress with an1800 s hold time.

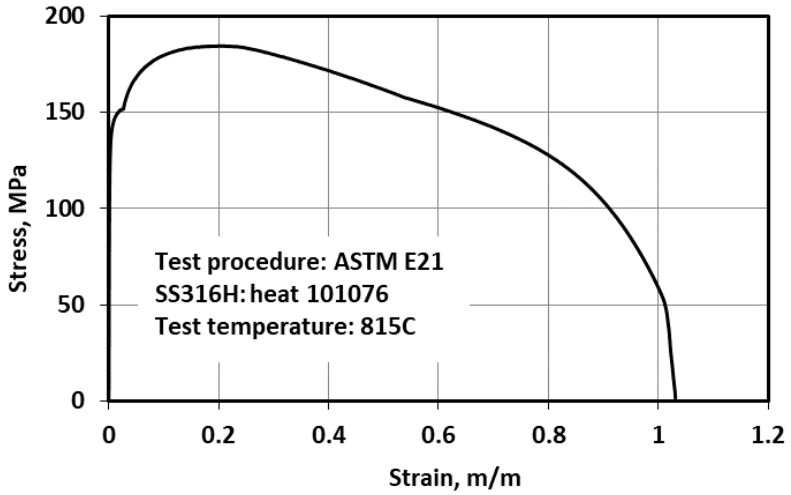

Fig. 23. Stress-strain curve of SS 316H (heat 101076) at 815ºC.

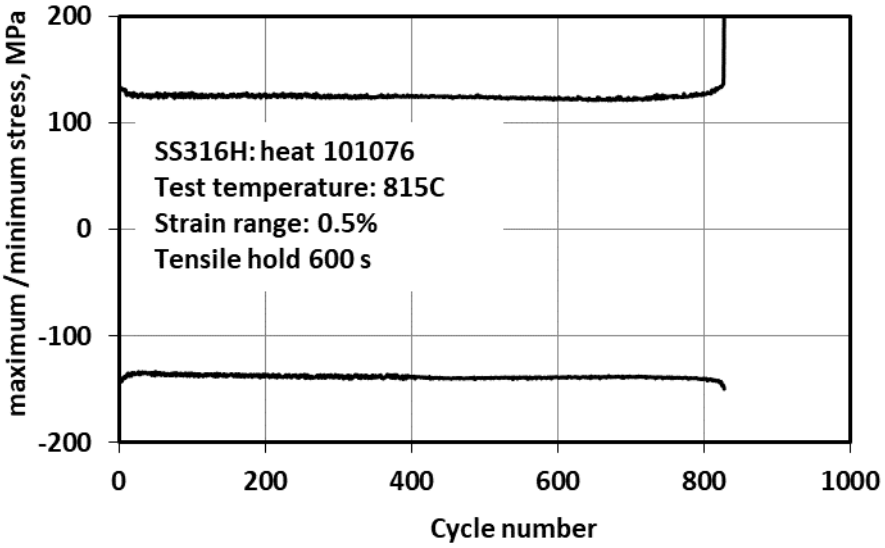

Fig. 24. Maximum and minimum stresses for SS 316H (heat 101076) tested at 0.5% strain range and 815ºC.

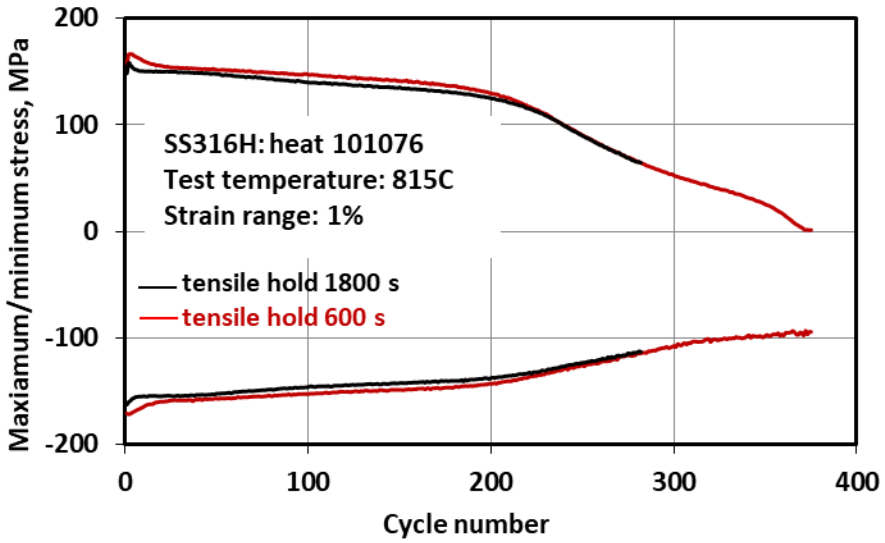

Fig. 25. Maximum and minimum stresses for SS 316H (heat 101076) tested at 1% strain range and 815°C.

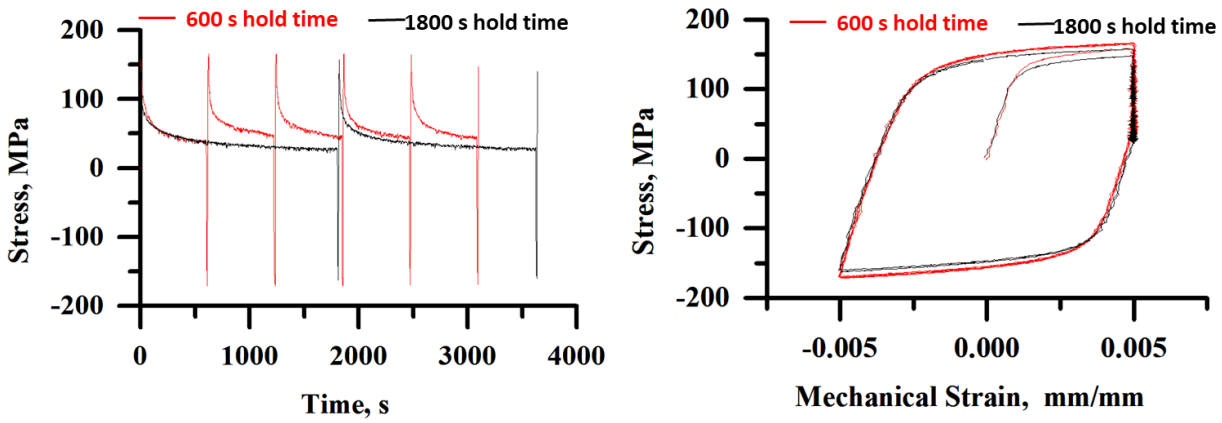

(a) (b)

Fig. 26. Stress histories (a) and hysteresis loops (b) of the initial cycles for SS 316H (heat 101076) with a 1% strain range and at 815°C.

Pure fatigue testing was performed at 427°C (800°F) on SS 316H (heat 101076), and the maximum and minimum stresses for 1% strain range testing are plotted in Fig. 27. The cycles to failure was 3000, indicating that this specific heat of SS 316H material is much stronger than the average code material fatigue property used to construct the design fatigue strain range in ASME SEC III Div. 5 Figure HBB-T-1420-1B.

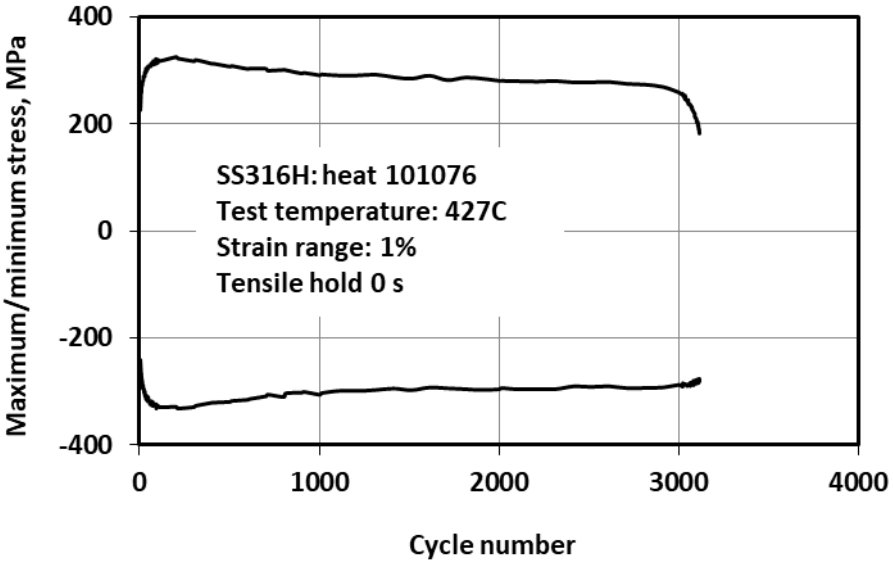

Fig. 27. Maximum and minimum stresses for SS 316H (heat 101076) tested at 1% strain range and 427°C.

Additionally, experimental data from thermomechanical fatigue provide useful information to validate the temperature-dependent parameters of the material constitutive model. Two thermomechanical fatigue tests were designed and performed on SS 316H (heat 101076) at temperature ranges of 675 to 815°C and 315 to 815°C with heating and cooling rates of 10°C/min using an igniter heater furnace. The specimen used had a standard creep fatigue specimen geometry, as shown in Fig. 10.

The temperature profile was controlled by a LabVIEW program. Prior to the thermomechanical fatigue test, the specimen was thermally cycled at zero load to collect thermal expansion measurement data. Thermomechanical fatigue was conducted according to standard test method ASTM-2368-10. It was under strain control with straining cycles that were 180 degrees out of phase with the thermal cycles (i.e., anti-phase thermomechanical fatigue). For this experiment, the total strain was controlled to be zero and the starting temperature. The relationship between the strain and the temperature for this anti-phase thermomechanical fatigue is schematically shown in Fig. 28.

The average thermal expansion coefficient was determined to be 21E-6 mm/mm/° C using a linear fit of the free expansion curves. The mechanical strain was calculated by subtracting the thermal expansion from the total strain. The strain range was 0.294% for the test at a temperature range of 675 to 815°C and 1.05% for a temperature range of 315 to 815°C. The strain rate was determined by the heating and cooling rates and was 3.5E-6 s^{-1}.

The thermal cycle profile, mechanical strain history, and the maximum and minimum stresses are plotted in Fig. 29 and Fig. 30. Representative hysteresis loops and the stress-vs.-temperature curves are presented in Fig. 31. The specimen was tested to failure for the large strain range test at a temperature range of 315 to 815°C with cycles to failure of 320. The test was interrupted at 600 cycles when it reached steady state for the temperature range 675 to 815°C. For both tests, the maximum tensile load was at the lowest temperature of the cycle and the maximum compressive load was at the highest temperature of the cycle. The ratio of the maximum tensile load to minimum compressive load was about 1.7 for the high-temperature range and 1.25 to 1.4 for the large temperature range of 315 to 815°C.

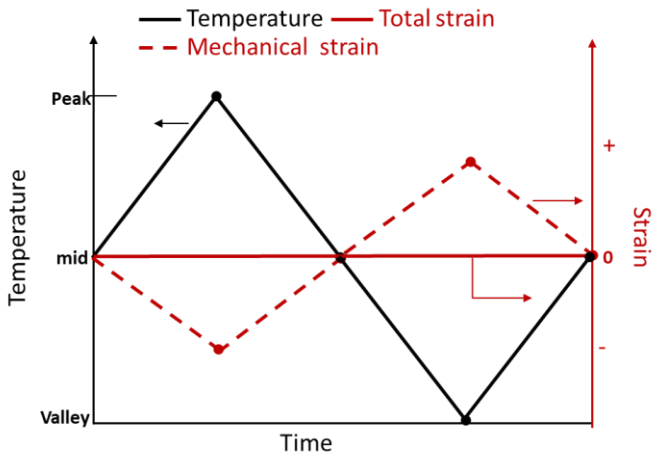

Fig. 28. Schematics of the anti-phase thermomechanical fatigue for one cycle.

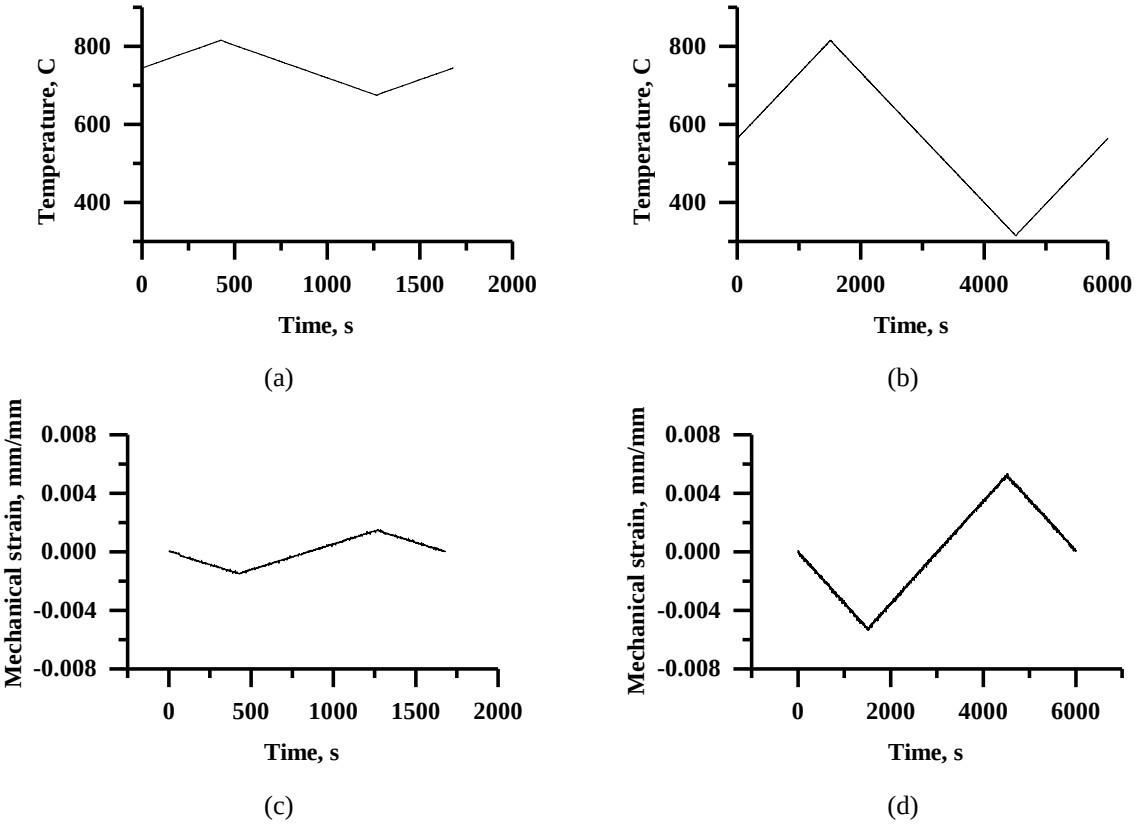

Fig. 29. Thermal cycle and mechanical strain of the thermo-mechanical fatigue on SS 316H at temperature ranges of 675 to 815°C (a, c) and 315 to 815°C (b, d).

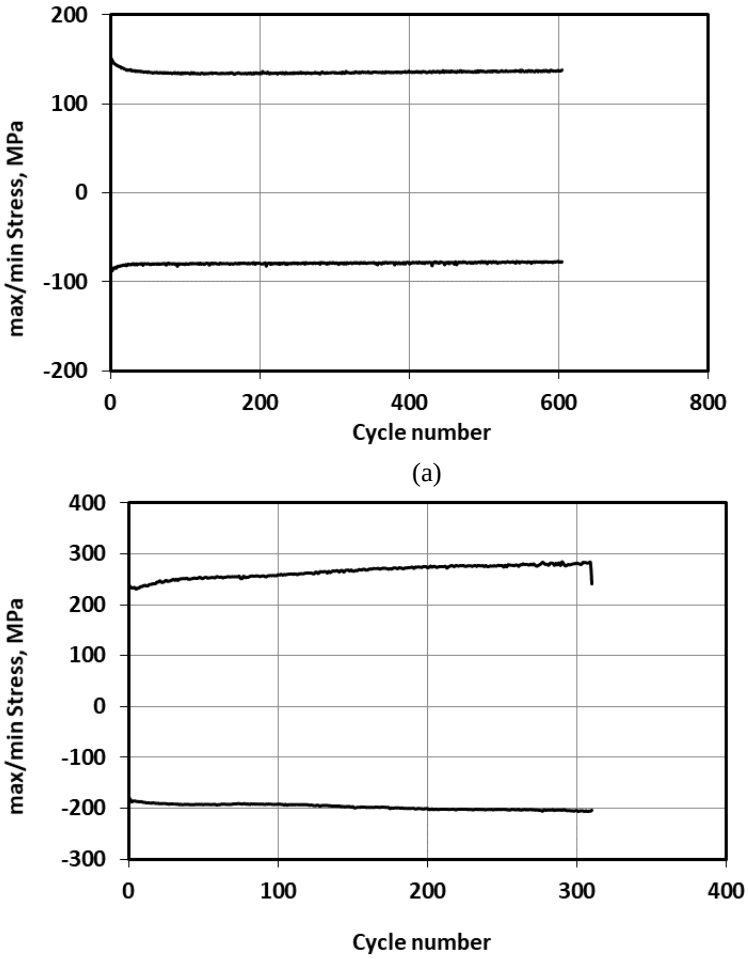

Fig. 30. Maximum and minimum stresses of the thermo-mechanical fatigue on SS 316H at temperature ranges of 675 to 815ºC (a) and 315 to 815ºC (b).

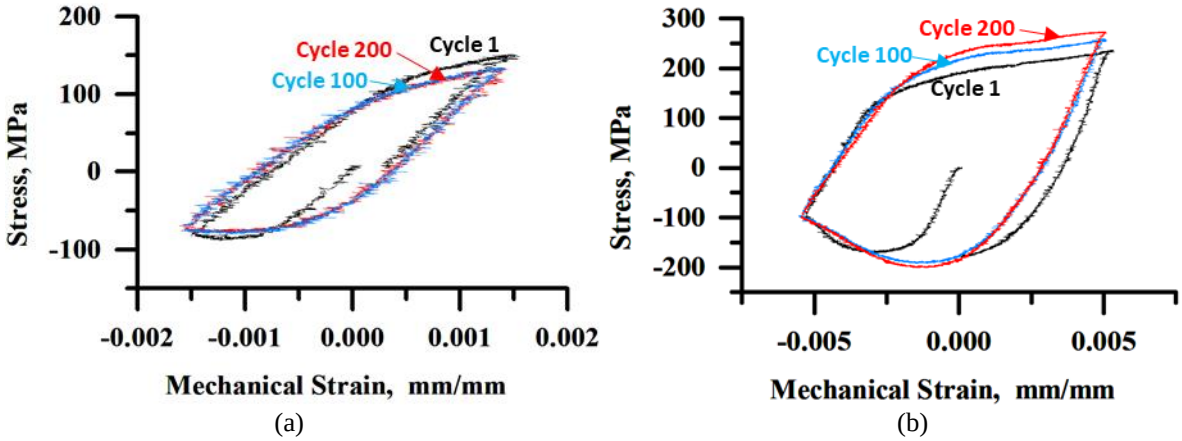

Fig. 31. Representative hysteresis loops of the thermo-mechanical fatigue on SS 316H at temperature ranges of 675 to 815ºC (a) and 315 to 815ºC (b).

6. SUMMARY

The experimental results in support of the development of the integrated EPP combined SMT creep-fatigue design methodology in FY 2019 are summarized in this report. The goal of the proposed approach is to combine the advantages of the EPP strain limits methodology, which avoids stress classification, with the advantages of the SMT method for evaluating CF damage without deconstructing the cyclic history into separate fatigue and creep damage evaluations.

The two-bar SMT and SBSMT methods were verified by designing and testing Alloy 617 and SS 316H at high temperatures. Both techniques capture the essential features of a test article with elastic follow-up and showed comparable results when the tests were designed for similar conditions. SBSMT is therefore considered to be the preferred technique in generating SMT test data base to support of the development of SMT-based design curves.

The role of the primary load on SMT CF life for Alloy 617 was evaluated at intermediate strain range using pressurized SMT at both 950^{o}C and 850^{o}C. The limited test results indicate that the primary load reduced the SMT CF life at 950^{o}C but not at 850^{o}C. Additional testing will be needed. The new concept of using pressurized SBSMT to evaluate the primary load effect has greatly simplified the testing program.

Additionally, selected mechanical tests were performed on SS 316H (heat 101076). The data were used to support the material constitutive model development for SS 316H.

REFERENCES

ASTM E21, “Standard Test Methods for Elevated Temperature Tension Tests of Metallic Materials”, ASTM International, West Conshohocken, PA.

ASMT E2714, “Standard Test Method for Creep-Fatigue Testing”, ASTM International, West Conshohocken, PA.

ASTM-E2368, “Standard Practice for Strain Controlled Thermomechanical Fatigue Testing”, ASTM International, West Conshohocken, PA.

ASTM-E606, “Standard Test Method for Strain-Controlled Fatigue Testing”, ASTM International, West Conshohocken, PA.

M. C. Messner, T. L. Sham, Y. Wang and R. I. Jetter (2018), “Evaluation of methods to determine strain ranges for use in SMT design curves”, ANL-ART-138, Argonne National Laboratory.

Wang, Y., Jetter, R. I., Krishnan, K., and Sham, T.-L, (2013a) “Progress Report on Creep-Fatigue Design Method Development Based on SMT Approach for Alloy 617”, ORNL/TM-2013/349, Oak Ridge National Laboratory, Oak Ridge, TN.

Wang, Y., Sham, T.-L, and Jetter, R. I., (2013b), “Progress report on the development of test procedure for the two-bar thermal ratcheting experiment for Alloy 617”, ORNL/TM-2013/318, Oak Ridge National Laboratory, Oak Ridge, TN.

Wang, Y., Jetter, R. I. and Sham, T.-L, (2014), "Application of Combined Sustained and Cyclic Loading Test Results to Alloy 617 Elevated Temperature Design Criteria", ORNL/TM-2014/294, Oak Ridge National Laboratory, Oak Ridge, TN.

Wang, Y., Jetter, R. I., Baird, S. T., Pu, C. and Sham, T.-L., (2015), "Report on FY15 Two-Bar Thermal Ratcheting Test Results", ORNL/TM-2015/284, Oak Ridge National Laboratory, Oak Ridge, TN.

Wang, Y., Jetter, R. I., and Sham, T.-L., (2016a), "FY16 Progress Report on Test Results In Support Of Integrated EPP and SMT Design Methods Development" ORNL/TM-2016/330, Oak Ridge National Laboratory, Oak Ridge, TN.

Wang, Y., Jetter, R. I., and Sham, T.-L., (2016b), "Preliminary Test Results in Support of Integrated EPP and SMT Design Methods Development", ORNL/TM-2016/76, Oak Ridge National Laboratory, Oak Ridge, TN.

Y. Wang, R. I. Jetter and T.-L. Sham, (2017a), "Report on FY17 Testing in Support of Integrated EPP-SMT Design Methods Development", ORNL/TM-2017/351, Oak Ridge National Laboratory, Oak Ridge, TN.

Wang, Y., Jetter, and Sham, T.-L., (2017b), "Pressurized Creep-Fatigue Testing of Alloy 617 Using Simplified Model Test Method", Proceedings of the ASME 2017 Pressure Vessels and Piping Conference, PVP2017-65457

Wang, Y., Jetter, R. I., Messner, M., Mohanty, S., and Sham, T.-L., (2017c), "Combined Load and Displacement Controlled Testing to Support Development of Simplified Component Design Rules for Elevated Temperature Service", Proceedings of the ASME 2017 Pressure Vessels and Piping Conference, PVP2017-65455

Wang, Y., Jetter, R. I., Messner, M., and Sham, T.-L., (2018), "Report on FY18 Testing Results in Support of Integrated EPP-SMT Design Methods Development", ORNL/TM-2018/887, Oak Ridge National Laboratory, Oak Ridge, TN.

Wang, Y., Jetter, R. I., Messner, M., and Sham, T.-L., (2019), " Development of Simplified Model Test Method for Creep-fatigue Evaluation", Proceedings of the ASME 2019 Pressure Vessels and Piping Conference, PVP2019-93648, July 2019, San Antonio, TX, USA